



AFRL-RZ-WP-TP-2012-0136

**EFFECTS OF LOCAL ARTIFICIAL DEFECTS IN
MULTIFILAMENTARY COATED CONDUCTORS WITH
PATTERNED LINKS (POSTPRINT)**

C. Kwon, J.L. Young, and R.G. James

California State University

George A. Levin, Timothy J. Haugan, and Paul N. Barnes

Mechanical Energy Conversion Branch

Energy/Power/Thermal Division

FEBRUARY 2012

Approved for public release; distribution unlimited.

See additional restrictions described on inside pages

STINFO COPY

© 2007 American Institute of Physics

**AIR FORCE RESEARCH LABORATORY
PROPULSION DIRECTORATE
WRIGHT-PATTERSON AIR FORCE BASE, OH 45433-7251
AIR FORCE MATERIEL COMMAND
UNITED STATES AIR FORCE**

REPORT DOCUMENTATION PAGE

Form Approved
OMB No. 0704-0188

The public reporting burden for this collection of information is estimated to average 1 hour per response, including the time for reviewing instructions, searching existing data sources, gathering and maintaining the data needed, and completing and reviewing the collection of information. Send comments regarding this burden estimate or any other aspect of this collection of information, including suggestions for reducing this burden, to Department of Defense, Washington Headquarters Services, Directorate for Information Operations and Reports (0704-0188), 1215 Jefferson Davis Highway, Suite 1204, Arlington, VA 22202-4302. Respondents should be aware that notwithstanding any other provision of law, no person shall be subject to any penalty for failing to comply with a collection of information if it does not display a currently valid OMB control number. **PLEASE DO NOT RETURN YOUR FORM TO THE ABOVE ADDRESS.**

1. REPORT DATE (DD-MM-YY) February 2012		2. REPORT TYPE Journal Article Postprint		3. DATES COVERED (From - To) 04 April 2005 – 04 April 2007	
4. TITLE AND SUBTITLE EFFECTS OF LOCAL ARTIFICIAL DEFECTS IN MULTIFILAMENTARY COATED CONDUCTORS WITH PATTERNED LINKS (POSTPRINT)				5a. CONTRACT NUMBER In-house	
				5b. GRANT NUMBER	
				5c. PROGRAM ELEMENT NUMBER 62203F	
				5d. PROJECT NUMBER 3145	
6. AUTHOR(S) C. Kwon, J.L. Young, and R.G. James (California State University) George A. Levin, Timothy J. Haugan, and Paul N. Barnes (AFRL/RZPG)				5e. TASK NUMBER 32	
				5f. WORK UNIT NUMBER 314532ZE	
				8. PERFORMING ORGANIZATION REPORT NUMBER AFRL-RZ-WP-TP-2012-0136	
7. PERFORMING ORGANIZATION NAME(S) AND ADDRESS(ES) California State University Department of Physics and Astronomy Long Beach, CA 90840				8. PERFORMING ORGANIZATION REPORT NUMBER AFRL-RZ-WP-TP-2012-0136	
Mechanical Energy Conversion Branch (AFRL/RZPG) Energy/Power/Thermal Division Air Force Research Laboratory, Propulsion Directorate Wright-Patterson Air Force Base, OH 45433-7251 Air Force Materiel Command, United States Air Force					
9. SPONSORING/MONITORING AGENCY NAME(S) AND ADDRESS(ES) Air Force Research Laboratory Propulsion Directorate Wright-Patterson Air Force Base, OH 45433-7251 Air Force Materiel Command United States Air Force				10. SPONSORING/MONITORING AGENCY ACRONYM(S) AFRL/RZPG	
				11. SPONSORING/MONITORING AGENCY REPORT NUMBER(S) AFRL-RZ-WP-TP-2012-0136	
12. DISTRIBUTION/AVAILABILITY STATEMENT Approved for public release; distribution unlimited.					
13. SUPPLEMENTARY NOTES Journal article published <i>Journal of Applied Physics</i> , Vol. 101, 2007. © 2007 American Institute of Physics. The U.S. Government is joint author of this work and has the right to use, modify, reproduce, release, perform, display, or disclose the work. PA Case Number: AFRL/WS 07-0739; Clearance Date: 04 Apr 2007. Work on this effort was completed in 2007. This paper contains color.					
14. ABSTRACT Multifilamentary coated conductor MFCC samples with patterned links have been studied using transport and scanning laser microscopy SLM techniques. Striation patterns are fashioned to define multiple filaments with discretely placed superconducting (SC) links between the filaments for current sharing and redistribution. After initial measurements, an artificial incision is made on a filament to mimic a disabled filament. The changes in global and local current transport characteristics are noted for in terms of the redistribution of current flow and the modification of local dissipation. Our results show that the patterned links between filaments play a vital role in redistributing current and encouraging current sharing. We find that the main factors in limiting the current-carrying capability of MFCC samples are local current density increases, which we call "current crowding." The susceptible areas for current crowding are several: 1. filaments adjacent to the disabled ones, since the intact filaments have to carry extra current, 2. the links where current redistribution occurs, and 3. the partially blocked filament.					
15. SUBJECT TERMS multifilamentary, coated conductor, dissipation, samples, superconducting, flow, filaments, transport, crowding, links					
16. SECURITY CLASSIFICATION OF:			17. LIMITATION OF ABSTRACT: SAR	18. NUMBER OF PAGES 12	19a. NAME OF RESPONSIBLE PERSON (Monitor) Timothy J. Haugan 19b. TELEPHONE NUMBER (Include Area Code) N/A
a. REPORT Unclassified	b. ABSTRACT Unclassified	c. THIS PAGE Unclassified			

Effects of local artificial defects in multifilamentary coated conductors with patterned links

C. Kwon,^{a)} J. L. Young, and R. G. James

Department of Physics and Astronomy, California State University, Long Beach, California 90840

George A. Levin, Timothy J. Haugan, and Paul N. Barnes

Propulsion Directorate, Air Force Research Laboratory, 1950 Fifth Street, Wright-Patterson Air Force Base, Ohio 45433-7919

(Received 27 August 2006; accepted 31 January 2007; published online 30 April 2007)

Multifilamentary coated conductor (MFCC) samples with patterned links have been studied using transport and scanning laser microscopy (SLM) techniques. Striation patterns are fashioned to define multiple filaments with discretely placed superconducting (SC) links between the filaments for current sharing and redistribution. After initial measurements, an artificial incision is made on a filament to mimic a disabled filament. The changes in global and local current transport characteristics are noted for in terms of the redistribution of current flow and the modification of local dissipation. Our results show that the patterned links between filaments play a vital role in redistributing current and encouraging current sharing. We find that the main factors in limiting the current-carrying capability of MFCC samples are local current density increases, which we call “current crowding.” The susceptible areas for current crowding are several: (1) filaments adjacent to the disabled ones, since the intact filaments have to carry extra current, (2) the links where current redistribution occurs, and (3) the partially blocked filament. © 2007 American Institute of Physics. [DOI: 10.1063/1.2716211]

I. INTRODUCTION

Second-generation high-temperature superconducting wires based on $\text{YBa}_2\text{Cu}_3\text{O}_7$ (YBCO), so-called coated conductors (CCs), have achieved dramatic improvements in current-carrying capability and in increasing the available length of wires. It is now possible to obtain a several meters long wire with $J_c > 10^6$ A/cm², which satisfies performance requirements for some applications.^{1,2} Rotating machinery, such as generators and motors, is one of the imminent applications considered for CCs.³ Since CCs will be exposed to ac magnetic fields, an important additional requirement in these applications is low ac loss. Due to the CC architecture, conventional solutions to reduce ac loss for wires cannot be employed in CCs. Hence, the challenge is to understand and ultimately to reduce ac loss in CCs.

The possible ac loss mechanisms are hysteretic loss, ferromagnetic loss of the substrate, eddy-current losses in the substrate and in the stabilizing layer, coupling loss between filaments, and transport-current losses. Since hysteretic loss is proportional to the width of the filament perpendicular to the applied field, the hysteretic loss poses a major problem in CCs due to the large geometric aspect ratio inherent to the architecture.

Several designs have been proposed in order to reduce ac loss.^{4–6} Carr and Oberly have proposed to divide the YBCO coated conductor cables into long filamentary strips with a little twist to reduce ac loss.⁴ The filamentary YBCO epitaxial films and CCs created by laser micromachining have been shown to reduce ac loss.^{7,8} However, without

some means to redistribute current in such geometry, a single defect in a filament will render a given filament useless over its whole length. One way to prevent such failures is to provide links or bridges between filaments. Research is underway to determine the best design for filaments and links, since the reduction of ac loss and current sharing are conflicting design requirements.^{6,9} Furthermore, feasibility, cost, stability, and quench protection are needed to be addressed for the final product.

One proposal is to cut the superconductor into parallel filaments and introduce periodic transverse crosscuts, where the crosscuts allow the magnetic flux to penetrate between the filaments and decouple them.⁵

Another proposal is to create a striation pattern to place the links, which could be normal metal or superconducting, in desired positions in order to reduce the transverse current.⁹ Superconducting (SC) links provide a better loss-sharing trade-off than normal-metal ones for moderate to high-frequency applications.⁶ Additional ac loss using the SC links is shown to be tolerable as long as the distance between the links is comparable to the length of the twist pitch.⁹ Several reports have demonstrated that the striated samples with interfilament links have lower ac losses than unstriated samples, even though the loss is higher than in fully striated samples without links.^{8,10–14} The interfilament links generally increase ac loss, and the degree of the increase depends on the placement and physical property of the links. Hence, the first consideration for the interfilament link design is the reduction of ac loss. Another important aspect of the design is to optimize current redistribution and sharing among filaments.

This paper addresses the issue of current sharing and

^{a)}Electronic mail: ckwon@csulb.edu

redistribution in multifilamentary coated conductors (MFCC) with patterned interfilamentary bridges when an artificial blockage, an incision, is created in a filament. Using scanning laser microscopy (SLM), we have obtained local maps of transport currents and superconducting dissipation.¹⁵ Our objectives are to study how disabled filaments modify local current transport, how it is reflected in local dissipation patterns, and how various striation patterns behave differently.

In this paper, several MFCC samples are studied before and after an incision is made to disable a filament. Each sample has multiple filaments with a different pattern of SC links. The links are created by laser micromachining to provide interfilamentary bridges. The samples are measured using conventional transport and SLM techniques. Our data shows that the interfilamentary links play a vital role in redistributing current among filaments. As transport currents redistribute at the links, the increased current density at these locations can cause premature dissipation. Also, an increased current density in filaments near a disabled one also makes them susceptible. We find that the local increases in current density, or current crowding, are the main sources in generating local dissipation and in limiting the current-carrying capability of MFCC samples, regardless of what striated pattern is used. A better design needs to be developed to minimize the local current crowding and reduce premature dissipation from the areas associated with links in disabled filaments as the current is redistributed to nearby intact filaments via the links.

II. EXPERIMENTAL DETAILS

All MFCC samples were provided by Air Force Research Laboratory. In the samples, the superconducting layer is divided into multiple filaments segregated by nonsuperconducting grooves. A sparse network of SC links between filaments is placed in the sample to facilitate current sharing. The samples are identified with the imposed pattern of interfilamentary links, i.e., zipper, brick wall, and fishnet patterns. Laser micromachining is used to create the striation patterns for filaments and links. Details on this method and information about magnetization loss measurements for the similar samples can be found in Ref. 11.

Each sample is prepared for four-probe transport measurements by depositing gold contacts. Special care has been taken to establish uniform gold coverage across the sample to ensure consistent electric contact among filaments. All MFCC samples in this paper have striations to the edges of the sample, and no precaution has been taken to restrict the current to the filaments. The current always flows along the filaments in this study, hence parallel to the striations. A portion of the current may flow in the substrate if the gold contacts establish an electrical connection in locations where the substrate lies exposed inside striations. However, this stray current does not affect the conclusions of this paper because SLM techniques measure current transport characteristics of the topmost superconducting layer. Our results also indicate that the current exchange between YBCO and the substrate occurs in the midway through filaments prob-

ably via melted and splashed Hastelloy substrate material, which provides the electrical connection between YBCO and the substrate.

Each sample is measured using conventional transport and SLM techniques. Detailed information about our SLM system can be found in earlier publications.^{15,16} We have used two modes of SLM: variable temperature scanning laser microscopy (VTSLM) and low temperature scanning laser microscopy (LTSLM). In VTSLM mode, a fixed bias current is applied (I_B) and SLM images are taken at varying temperatures near the superconducting transition. The spatial distribution of superconducting transition temperature T_c and the current distribution can be extracted from VTSLM images. In the LTSLM mode, the sample temperature is fixed at $T < T_c$ and SLM images are taken while the bias current is increased above I_c . LTSLM images provide the superconducting dissipation map of the sample. For more information about LTSLM, see a detailed review paper in Ref. 18.

After initial transport and SLM measurements, the sample is removed from the cryostat and an incision is made to disable a filament. The incision is made using a LaserScissors Pro 300 workstation from Cell Robotics Inc., which employs a nitrogen-pumped UV laser for cutting. After the incision is made, the sample is returned to the cryostat and characterized again using transport and SLM measurements.

III. RESULTS AND DISCUSSIONS

The experimental results and discussions will be presented in the next four sections. First, we will explain what information we can get from VTSLM images and compare it with the results of transport measurements in MFCC samples. In Sec. III B, a comparative SLM study of before and after cuts will be presented for a fishnet pattern sample. In Sec. III C, we will discuss the origin of visible or a lack of features in SLM images. In Sec. III D, the results from different striated patterns and future direction will be discussed.

A. VTSLM images and transport measurements

Figures 1(a) and 1(b) are the resistive transition and series of I - V characteristics measured from a zipper pattern sample shown in the insert of Fig. 1(a). The resistive transition shows a double drop in resistance, which indicates spatial inhomogeneity of T_c . I - V curves are clearly nonlinear below 90.0 K.

Figures 1(c)–1(j) are series of VTSLM images taken at $I_B=40$ mA with increasing temperature. The solid dots in Fig. 1(a) show the temperatures where VTSLM images are taken for Figs. 1(c)–1(j). The insert in Fig. 1(a) is a photodiode image acquired simultaneously with the VTSLM images. The gold electrodes are just outside of the viewing area, but they are placed to ensure the current flow along the filaments. The VTSLM image is a plot of δV , the voltage response of the sample due to the laser, and the intensity of δV is shown in the gray color scale.

The series of VTSLM images, Figs. 1(c)–1(j), show that δV shifts from the right to the left side of the sample with increasing temperature. The left side of the sample (2/3 of

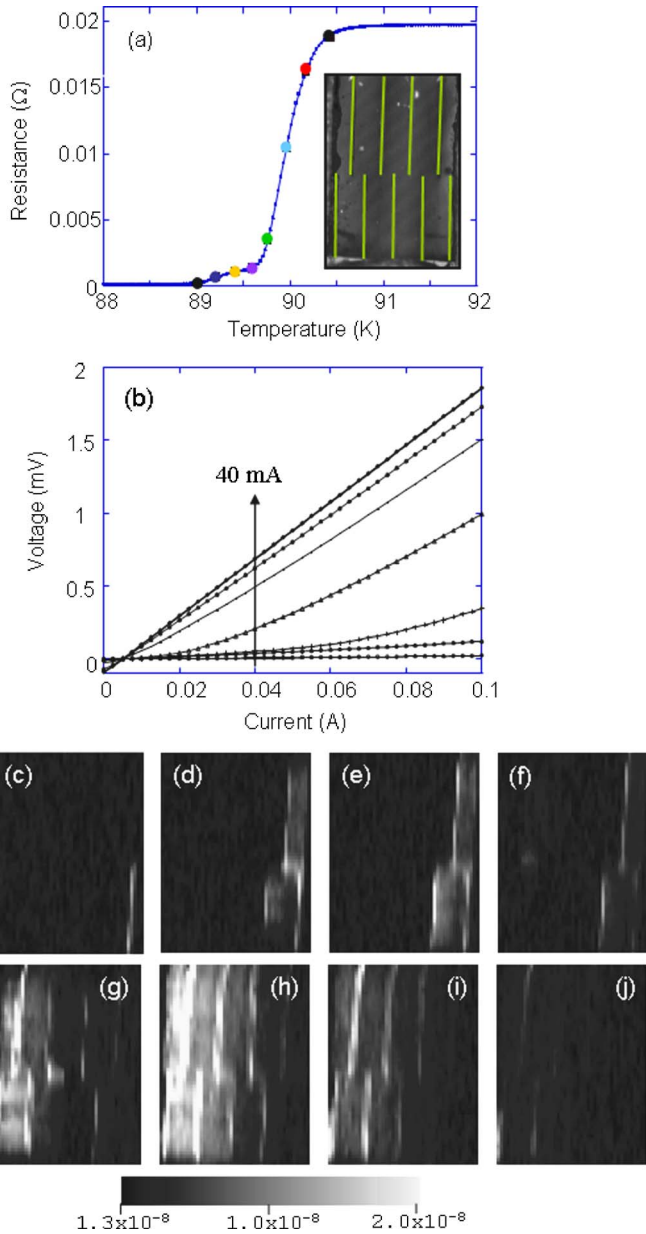


FIG. 1. (a) Resistive transition of a zipper pattern striated sample. (Insert) Photodiode image of the sample. The thin lines are the striations separating the filaments shown as large stripes. The width of each filament is 1.0 mm, and the offset distance between rows of filaments is 0.5 mm. The current flows along the filaments. (b) I - V characteristics of the sample measured at 91.0, 90.4, 90.2, 90.0, 89.8, 89.6, and 89.0 K. [(c)–(j)] VTSLM images taken at $I_B=40$ mA from the area shown in the insert of (a). Scan area is 4.5×6.0 mm² with 100 μ m resolution.

the total scanned area) exhibits a maximum δV at 90.0 K [Fig. 1(h)], while the two right-side filaments show the strongest δV at 89.4 K [Fig. 1(e)].

In our earlier publication, we have reported that a maximum δV is observed where the sharpest drop in the resistance (the maximum $\partial R/\partial T$) occurs.¹⁶ At 90.0 K where the major drop in resistance occurs, most of the sample has a maximum δV , as seen in Fig. 1(h). On the other hand, the two right-side filaments have a maximum δV at 89.4 K, the same temperature at which the secondary drop in resistance is observed. We conclude that the double drop in resistance occurs because there are two distinct superconducting tran-

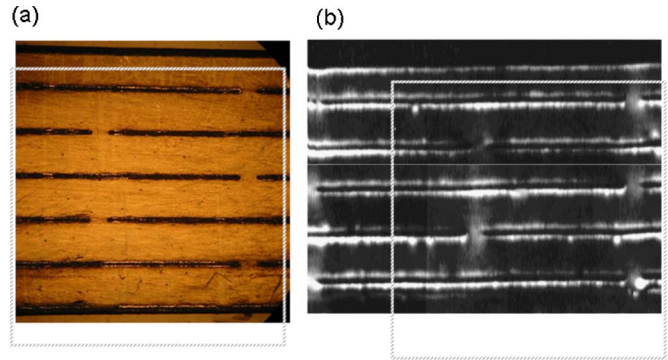


FIG. 2. (a) A photograph of a brick wall pattern striated sample. The width of each filament is 250 μ m, and the link opening between filaments is 125 μ m. (b) A VTSLM image from the sample using 10 μ m resolutions. The box is drawn over the same area for (a) and (b).

sition areas in the sample. VTSLM images help us to identify the local areas responsible for the double resistive transition.

As shown in Fig. 1(b), I - V begins to deviate from Ohmic behavior at 90.2 K, and I_c can be clearly determined below 90.0 K. Since VTSLM images were taken at a fixed current ($I_B=40$ mA), some images were obtained while I - V characteristics were no longer linear. Hence, one can expect the map of superconducting dissipation to be similar to the VTSLM images taken at lower temperatures. This subject will be discussed further in the next section.

Another noticeable feature from the VTSLM images in Fig. 1 is the distinct appearance of striations. This characteristic is shared among all MFCC samples we studied with SLM.

If we use a high resolution SLM image, it is easier to explain why the striations appear as distinctly as they do. Figure 2(a) is a photograph of a brick wall pattern MFCC sample, where the micromachined striations are seen as thick dark lines. Figure 2(b) is a high resolution VTSLM image taken at the temperature when $\partial R/\partial T$ is the greatest. Figure 2 shows that δV is stronger at the edges than in the central region of a filament. Hence, the striations are outlined by the large δV along their sides, making them easy to recognize. Especially in lower resolution, this outlining effect is responsible for the distinct appearance of striations.

The laser micromachining process creates a deep trench of about 30 μ m wide to the substrate by ablating YBCO and other materials.¹¹ Hence, little or no current flows within striations since these regions are nonsuperconducting. Figure 2(b) clearly shows no δV inside the striations confirming the lack of current flow.

We believe that the relatively stronger δV along the edges of a filament is due to the usual distribution of current density in the mixed-state superconductor rather than some kind of nonuniformity. The possibility of inhomogeneous T_c distribution is considered and discarded, since VTSLM images show no discernible T_c inhomogeneity across the filament. A theoretical analysis of the critical-state model of infinitely long type-II superconducting thin films shows that higher density current flows along the edges of a film when compared to the center of a film.¹⁷ Unlike an infinitely thick slab where the current flows within a penetration depth (λ)

and decays exponentially, transport current flows not only along the edges but also across the entire width of the film. Since VTSLM images are taken at temperatures with nonlinear I - V as discussed earlier, the theoretical model provides a plausible explanation for the relatively larger δV at the edges of a filament.

One more thing to note in Fig. 2 is that each filament appears to carry similar amounts of current with similar spatial distribution patterns. The outer filaments do not carry higher currents than the middle ones.

The combination of high δV along the striation and low δV inside the filaments makes each striation a landmark in SLM images and helps us to locate and identify features in our study. The breaks in striations, created to provide the interfilamentary bridges or links, appear to have fairly strong δV in Fig. 2(b); δV in this region is larger than in the center of filaments and smaller than at the edges. By interpreting the intensity of δV to be representative of local current density, we conclude that current flows through the links and the links enable the redistribution of current among filaments as intended. However, this mechanism also implies that the current density at/near the links can be high. Our earlier study of MFCC samples has shown that the interfilamentary link area is likely to create early dissipation.¹⁵ The premature dissipation at the links is caused mainly by current crowding. Any blockage in a filament will increase the current density at the links (as intended), and the increased current density can exceed the local critical current since the links already carry higher current.

In the studied MFCC striated samples, the interfilamentary link is nominally half of the filament width with an expectation that the link can handle the redirected current since there is one on each side of a filament. However, our results suggest that larger current density along the filament edges adds more constraints in the design of an optimal pattern of links, namely, their width and placement.

B. Before and after a cut

A fishnet pattern sample was measured before and after two filaments had been cut with our LaserScissor system. Figure 3(a) is a photograph taken after the cuts. Figures 3(b)–3(e) show VTSLM and LTSLM images taken before and after the cuts. VTSLM images are taken at the temperature where $\partial R/\partial T$ is a maximum, and LTSLM images are taken at 0.5 K below T_c . Most striations can be identified by the stronger δV along them, which is enhanced in the image due to a low spatial resolution as discussed earlier. We first note that in all Figs. 3(b)–3(e) the δV is visible in the upper rows of filaments; we postpone the discussion of this effect to the next section.

SLM images are clearly different before and after the cuts are made. VTSLM images of the original sample shows that two filaments (T3 and T4), which will be cut, are clearly visible and are carrying current in Fig. 3(b). T3 and T4 are chosen because LTSLM image [Fig. 3(c)] shows dissipation in those filaments before any other filaments.

After they are cut, VTSLM images [Fig. 3(d)] show that T3 and T4 exhibit no δV while the neighboring filaments

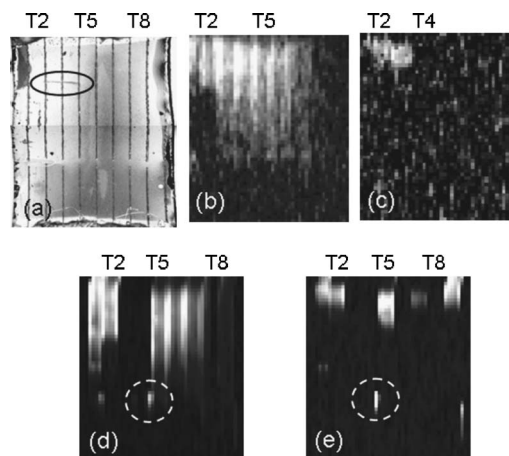


FIG. 3. (a) A photograph of a fishnet pattern striated sample. The width of filaments is $500\ \mu\text{m}$ with link openings of $300\ \mu\text{m}$. The circle marks the incision made to cut two filaments. (b) and (c) are VTSLM and LTSLM images, respectively, taken before the cut with $100\ \mu\text{m}$ resolution. After-cut images are shown in (d) VTSLM and (e) LTSLM.

(T1, T2, and T5) have a stronger signal indicating that the current from the cutoff filaments has been channeled to the neighboring filaments increasing their current density. The LTSLM image of Fig. 3(e), taken after the cuts were made in T3 and T4, shows that the dissipation occurs in neighboring filaments (T1, T2, and T5) since they are now carrying higher current density than other filaments.

One more thing we note from the after cut images is the area marked with dotted circles in Figs. 3(d) and 3(e), δV around the SC links connecting top and bottom rows of filaments. Figure 3(d) shows strong δV in several links as compared to the before cut VTSLM image in Fig. 3(b), confirming the increased current density at the links. In addition, LTSLM in Fig. 3(e) shows strong dissipation at one of the links near the cutoff filament (T4) indicating the increased current density in this specific link. This increase in current density during the current redistribution causes the link to be a region of early dissipation.

In summary, interfilamentary bridges redistribute current and allow current sharing among filaments. However, the increased current density around the disabled filaments can cause current crowding at the links as well as in adjacent filaments. This is the main source of early dissipation. Future designs of striation patterns should consider this issue.

C. Understanding features in SLM images

Understanding the cause of a feature from a single SLM image is a difficult task. The interpretation of the data requires taking a comprehensive set of VTSLM and LTSLM images. As an example, a small δV can be due to (a) small or no local current $J(x, y)$ or (b) broad superconducting transitions with small $\partial R/\partial T$ or $\partial J_c/\partial T$.^{18–20} The small or no local current can stem from the sample geometry (for example, a wider section of a sample has lower current density²⁰), from various material issues (such as current percolation,²¹ artificial defects,²² discontinued YBCO on the laminated buffer layer,²³ or other macroscopic defects), or from nonuniform contact with individual filaments in MFCC samples.

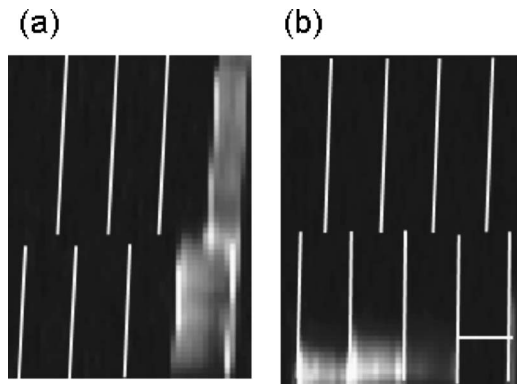


FIG. 4. (a) LTSLM image of the zipper pattern sample shown in Fig. 1 taken at $I_B=120$ mA and at 0.5 K below T_c . (b) LTSLM image of the same sample after an incision was made to cut a filament. The overlaid pattern shows the location of striations and the cut.

In Fig. 3, δV in the bottom rows of filaments is within the noise level and indiscernible, while visible features are concentrated at the top rows. Since there is no indication of a disabled filament or material imperfection, current seems to be uniformly carried by all bottom filaments. We postulate that the current density is smaller in the bottom rows than the top rows of filaments, because one of the top filaments (T8) appears not to carry any current. Indeed, no δV emerges in T8 even after two filaments were cut and current density was increased in other top filaments. The absence of current in T8 can be caused by material defects in T8 or a bad contact. Since T8 is not carrying current, the current density at the other top filaments must be higher than the bottom ones. This provides a plausible explanation for why only the top rows of filaments are visible in Fig. 3.

As we observed earlier, the interfilamentary bridges provide important pathways for current redistribution. In addition, we find evidence from our data that some current may leak to the substrate. Figure 3(d) shows a strong δV in T2 (the nearest neighbor filament to the cutoff ones), but δV decreases quickly before the current reaches the interfilamentary links. This suggests current leakage midway through the filament. Reference 11 reported that the laser micromachining process causes the Hastelloy substrate to melt and splash, the splash can establish an electrical connection between YBCO and the substrate in some parts of the grooves. They found that the electrical contact between Hastelloy substrate and YBCO-Ag due to Hastelloy splash is partly responsible for the increased ac loss in similarly prepared MFCC samples. Hence, we believe that the same kind of electrical contact due to Hastelloy splash may be responsible for the observed current leakage in our samples.

As shown in Figs. 3(a) and 3(b), there is no resemblance between the VTSLM image taken where $\partial R/\partial T$ is a maximum and the LTSLM image showing the local dissipation in superconducting state. On the other hand, LTSLM images look a lot like the VTSLM images taken at lower temperature when the resistance is close to zero and I - V is nonlinear. Figure 4(a) is a LTSLM image of the zipper pattern sample shown in Fig. 1 taken at $I_B=120$ mA. Figure 4(a) looks similar with Fig. 1(d) where only the lower T_c area is visible even though Fig. 1(d) is taken with $I_B=40$ mA. We conclude that

the lower T_c section of the sample dominates dissipation at this temperature. One can reasonably think that a set of VTSLM images not only provides information about T_c distribution and local current flow¹⁵ but also gives a glimpse of the local dissipation pattern.

D. Comparison of different interfilamentary link patterned samples

Figure 4(b) is a LTSLM image of the zipper pattern sample shown in Fig. 1 after an incision was made to one of the filaments. The cut was intentionally made on the bottom filament with lower T_c . The resistive transition still shows the secondary resistance drop at lower temperature, even though it is not as distinct as Fig. 1(a) because of the intact upper filament with lower T_c , as seen in Fig. 1(d).

Similar to Fig. 3 in the fishnet pattern sample, the cutoff filament does not carry any current, which we deduce from the absence of a δV . The intact bottom filaments appear clearly in the LTSLM image [Fig. 4(b)] indicating an increased current density. This is the likely culprit for the early dissipation.

In this sample, we do not find any evidence of early dissipation at the interfilamentary links. This lack of an effect at the links may indicate the superiority of the zipper pattern relative to other patterns. An alternative explanation for no dissipation at the links can be current leakage. The sudden disappearance of δV in the midway through the bottom filaments [Fig. 4(b)] may suggest current leakage via Hastelloy splash as we discussed earlier.

Oxygen annealing after the laser micromachining oxidizes Hastelloy splash in the striations, breaking the electrical connection between the substrate and YBCO-Ag. Results from the annealed samples will also provide a fair comparison among different patterns, which is not mired by current leakage. Hence, we plan to study annealed samples. On the other hand, one may be able to take advantage of current leakage since it provides an innate way to redistribute current. Further research is needed to investigate this possibility.

Figure 5(a) is a LTSLM image from a brick wall pattern sample after a laser cut. The LTSLM image is overlaid on a photodiode image taken simultaneously in Fig. 5(c). The two strong signals around the cut are the most distinctive feature in VTSLM and LTSLM images after the cut. One explanation is that the laser cut did not sever the filament over its whole width. The narrow path in the filament at the edge of the cut causes high current density, which is added to the current density already enhanced along the edges of the filament. The incomplete cut can cause the current density to easily exceed the local critical current. Hence, it becomes the most dominant feature in the sample. The two dots are the only visible features in all SLM images taken after the cut. It is easy to imagine a local temperature increase due to the two hot spots, and therefore, they can be a possible cause for catastrophic failure of the sample.

IV. SUMMARY

Using transport and SLM measurements, we studied 5 multifilamentary coated conductor (MFCC) samples with

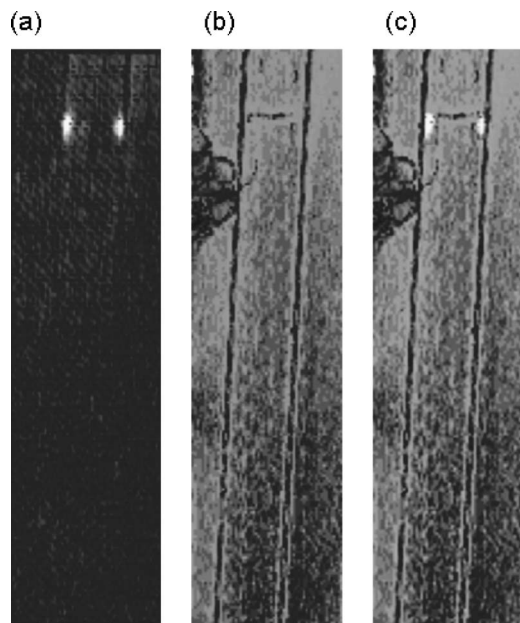


FIG. 5. (a) LTSLM image from a brick wall pattern striated sample after the cut. The image is taken with $20\ \mu\text{m}$ resolution. The sample consists of eight $500\ \mu\text{m}$ wide filaments, but only this area shows discernible SLM signal after the cut. (b) A photodiode image taken simultaneously. (c) LTSLM image overlaid on the photodiode image.

various patterned superconducting links. As expected, the interfilamentary bridges redistribute the current and enables current sharing among filaments. Our experiments show that the main dissipation mechanism is a local increase in current density, or current crowding, caused by disabled/defective filaments. The susceptible areas for current crowding are the intact filaments adjacent to the faulty ones that have to carry extra current, the links where current redistribution occurs, and the partly blocked filament. Hence, future design of the striated pattern needs to consider the minimization of local current crowding in addition to the reduction of ac loss. Our results indicate that the zipper pattern might be less susceptible for the current crowding than other patterns. Further study is needed using oxidized samples and varying the physical design parameters such as the ratio between the filament width and the link width, the distance between the rows of filaments, and the width of filaments.

ACKNOWLEDGMENTS

We would like to thank Megumi Yamamoto for help in preparing the figures and Dr. Kenealy and Dr. Bill for the critical reading of the manuscript. This work was supported by the Air Force Office of Science Research under Grant No. FA9550-05-1-0037 and by the SCAC awards at CSULB. The LaserScissor workstation is funded through National Science Foundation Grant No. DBI-0421441.

¹V. Selvamanickam *et al.*, IEEE Trans. Appl. Supercond. **15**, 2596 (2005).

²A. P. Malozemoff, J. Mannhart, and D. Scalapino, Phys. Today **58**(4), 41 (2005).

³P. N. Barnes, M. D. Sumption, and G. L. Rhoads, Cryogenics **45**, 670 (2005).

⁴W. J. Carr and C. E. Oberly, IEEE Trans. Appl. Supercond. **9**, 1475 (1999).

⁵S. P. Ashworth and F. Grilli, Supercond. Sci. Technol. **19**, 227 (2006).

⁶P. N. Barnes and M. D. Sumption, J. Appl. Phys. **96**, 6550 (2004).

⁷C. B. Cobb, P. N. Barnes, T. J. Haugan, J. Tolliver, E. Lee, M. Sumption, E. Collings, and C. E. Oberly, Physica C **382**, 52 (2002).

⁸N. Amemiya, S. Kasai, K. Yoda, Z. N. Jiang, G. A. Levin, P. N. Barnes, and C. E. Oberly, Supercond. Sci. Technol. **17**, 1464 (2004).

⁹G. A. Levin and P. N. Barnes, IEEE Trans. Appl. Supercond. **15**, 2819 (2005).

¹⁰M. Majoros, B. A. Glowacki, A. M. Campbell, G. A. Levin, P. N. Barnes, and M. Polak, IEEE Trans. Appl. Supercond. **15**, 2 (2005).

¹¹G. A. Levin, P. N. Barnes, N. Amemiya, S. Kasai, K. Yoda, Z. A. Jiang, and A. Polyanskii, J. Appl. Phys. **98**, 113909 (2005).

¹²G. A. Levin, P. N. Barnes, N. Amemiya, S. Kasai, K. Yoda, and Z. Jiang, Appl. Phys. Lett. **86**, 072509 (2005).

¹³P. N. Barnes, G. A. Levin, C. Varanasi, and M. D. Sumption, IEEE Trans. Appl. Supercond. **15**, 2827 (2005).

¹⁴M. Polak, E. Demencik, L. Jansak, P. Mozola, D. Aized, C. L. H. Thieme, G. A. Levin, and P. N. Barnes, Appl. Phys. Lett. **88**, 232501 (2006).

¹⁵L. B. Wang, P. Selby, C. Khanal, G. Levin, T. J. Haugan, P. N. Barnes, and C. Kwon, IEEE Trans. Appl. Supercond. **15**, 2950 (2005).

¹⁶L. B. Wang, M. B. Price, J. L. Young, C. Kwon, T. J. Haugan, and P. N. Barnes, Physica C **405**, 240 (2004).

¹⁷E. Zeldov, J. R. Clem, M. Mcelfresh, and M. Darwin, Phys. Rev. B **49**, 9802 (1994).

¹⁸A. P. Zhuravel, A. G. Sivakov, O. G. Turutanov, A. N. Omelyanchouk, S. M. Anlage, A. Lukashenko, A. V. Ustinov, and D. Abraimov, Low Temp. Phys. **32**, 592 (2006).

¹⁹R. Gross and D. Koelle, Rep. Prog. Phys. **57**, 651 (1994).

²⁰D. Abraimov, D. M. Feldmann, A. A. Polyanskii, A. Gurevich, G. Daniels, D. C. Larbalestier, A. P. Zhuravel, and A. V. Ustinov, Appl. Phys. Lett. **85**, 2568 (2004).

²¹L. B. Wang, G. You, K. R. Barraca, K. Waller, J. M. Mahoney, J. L. Young, and C. Kwon, IEEE Trans. Appl. Supercond. **15**, 3676 (2005).

²²D. V. Abraimov *et al.*, IEEE Trans. Appl. Supercond. **15**, 2954 (2005).

²³T. Kiss, IEEE Trans. Appl. Supercond. (to be published).